J. Fluid Mech. (1989), *vol.* 203, *pp.* 381–400
Printed in Great Britain

The squeezing of red blood cells through capillaries with near-minimal diameters

By D. HALPERN AND T. W. SECOMB
Program in Applied Mathematics and Department of Physiology, University of Arizona, Tucson, AZ 85724, USA

(Received 19 May 1988 and in revised form 5 January 1989)

An analysis is presented of the mechanics of red blood cells flowing in very narrow tubes. Mammalian red cells are highly flexible, but their deformations satisfy two significant constraints. They must deform at constant volume, because the contents of the cell are incompressible, and also at nearly constant surface area, because the red cell membrane strongly resists dilation. Consequently, there exists a minimal tube diameter below which passage of intact cells is not possible. A cell in a tube with this diameter has its critical shape: a cylinder with hemispherical ends. Here, flow of red cells in tubes with near-minimal diameters is analysed using lubrication theory. When the tube diameter is slightly larger than the minimal value, the cell shape is close to its shape in the critical case. However, the rear end of the cell becomes flattened and then concave with a relatively small further increase in the diameter. The changes in cell shape and the resulting rheological parameters are analysed using matched asymptotic expansions for the high-velocity limit and using numerical solutions. Predictions of rheological parameters are also obtained using the assumption that the cell is effectively rigid with its critical shape, yielding very similar results. A rapid decrease in the apparent viscosity of red cell suspensions with increasing tube diameter is predicted over the range of diameters considered. The red cell velocity is found to exceed the mean bulk velocity by an amount that increases with increasing tube diameter.

1. Introduction

The aim of this paper is to develop theoretical models for the motion of elongated rigid and flexible particles along tubes, when particle diameters are comparable with tube diameters. This work is motivated by an interest in the flow of red blood cells in microvessels. In large vessels, such as arteries and veins, blood can be represented as a continuum, but in microvessels the particulate nature of blood must be considered. Fahraeus & Lindqvist (1931) showed that the apparent viscosity of blood in microvessels decreases with decreasing vessel diameter. Gaehtgens (1980), using human blood, demonstrated that this reduction continues down to capillaries with diameters of 4 to 5 μm. However, the apparent viscosity increases for vessels with diameters less than this, and tends to infinity as a critical diameter is reached. This is the minimal vessel size that allows a cell to pass without increasing its surface area. It has long been stated that the cell shape in this critical case is a cylinder with two hemispherical ends (Canham & Burton 1968). This may be verified using the calculus of variations, by seeking to minimize the vessel radius while satisfying the constraints of constant cell volume V and surface area A. For typical human cells

($V = 90\ \mu m^3$, $A = 135\ \mu m^2$), the critical radius r_c is 1.42 μm and the length l_c of the cylindrical part is 12.26 μm.

Theoretical models to describe the motion of red blood cells can be formulated from first principles, since extensive experimental work has been carried out to determine the mechanical properties of red blood cells. The fluid mechanics of the suspending plasma must also be considered. Several approximations can be made since the plasma is an incompressible Newtonian fluid, and since inertial effects are negligible. The existence of a thin plasma layer between the vessel and membrane walls suggests that the Navier–Stokes equations can be approximated by those of lubrication theory. Experimental observations show that as the capillary radius decreases, the red cells become longer and narrower and have approximately axisymmetric shapes.

Secomb *et al.* (1986) developed asymptotic and numerical solutions for the motion of axisymmetric red blood cells in capillaries, using lubrication theory. Here, analogous methods are used to analyse red cell motion in narrower capillaries, with near-minimal diameters. In §2 the governing equations of membrane equilibrium and fluid mechanics are established. Section 3 is devoted to asymptotic and numerical solutions for near-critical cell shapes which correspond to the high-velocity limit, and §4 to solutions for less elongated red blood cells. In §5 the equations derived in §2 are solved numerically, and the results are compared to the predictions of §§3 and 4 and to other analyses. This model has essentially three free parameters: the sphericity index

$$I_S = \frac{4\pi}{A}\left[\frac{3V}{4\pi}\right]^{\frac{2}{3}}, \tag{1.1}$$

the vessel radius, and the cell velocity. Solutions for cells with different sphericities are presented here since red blood cells may have a wide range of volumes and surface areas (Papenfuss & Gross 1981).

2. The governing equations

2.1. *Membrane equilibrium*

The red blood cell consists of a thin elastic membrane filled with cytoplasm, which is an incompressible Newtonian fluid. Under steady conditions only elastic resistance to deformations needs to be considered. The modulus of shear elasticity (4.2×10^{-3} dyn/cm) is much smaller than that of isotropic dilation (500 dyn/cm). Thus isotropic tension which tends to increase the area of the membrane encounters a stiff elastic resistance but, at the same time, the membrane shears readily. The bending modulus (1.8×10^{-12} dyn cm) is also very small and consequently bending resistance is significant only in regions of high curvature.

The external fluid forces are balanced by membrane-induced stresses. When the membrane is highly stressed, shear and bending strains must be very large in order to generate correspondingly large shear and bending resistances, but small membrane dilations can generate high isotropic tensions. In vessels with near-minimal diameters, large external viscous shear stresses are therefore balanced primarily by isotropic tensions. We refer to this as the high-velocity limit. Shear and bending resistances become increasingly important at low cell velocities.

Following Secomb *et al.* (1986), we introduce cylindrical coordinates (σ, ϕ, z) as shown in figure 1. It is convenient to identify points on the membrane surface in terms of s, the arclength in a plane containing the axis, and ϕ, the azimuthal angle.

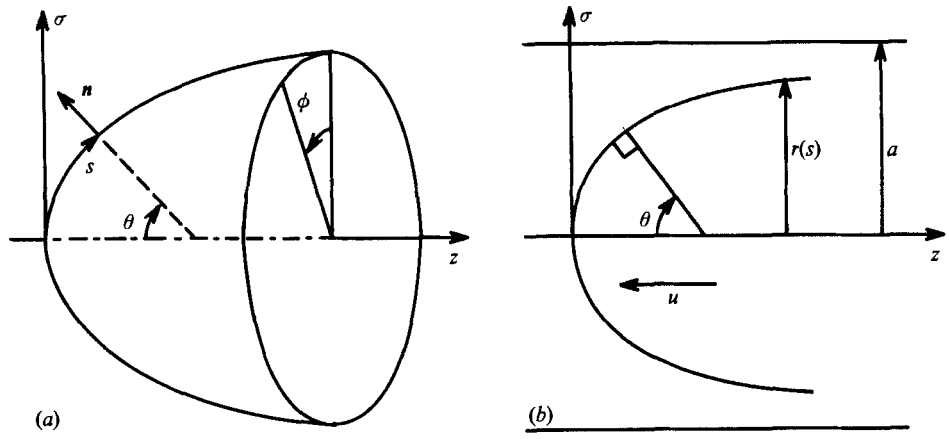

FIGURE 1. Variables describing geometry of an axisymmetric red blood cell in a cylindrical tube.

Also we define $r(s)$, the distance from the axis; $\theta(s)$, the angle that the vector $\boldsymbol{n}$ normal to the surface makes with the z-axis; $k_\phi(s)$ and $k_s(s)$, the principal curvatures; $m_s(s)$ and $m_\phi(s)$, the bending moments; $t_s(s)$ and $t_\phi(s)$, the membrane tensions; and $q_s(s)$, the shear force per unit length. The subscripts s, ϕ represent components in the coordinate directions. The components of tension are

$$t_s = t_m + t_d, \quad t_\phi = t_m - t_d, \tag{2.1}$$

where

$$t_d = \tfrac{1}{2}\kappa\,(\lambda_s^2 - \lambda_s^{-2}) - \tfrac{1}{2}B(k_s - k_\phi)\,(k_s + k_\phi - k_0), \tag{2.2}$$

in which the interaction between bending and tension forces is included (Secomb 1988). Here $t_m(s)$ denotes the mean tension, κ is the shear modulus of the membrane, $\lambda_s = \mathrm{d}s/\mathrm{d}s_0 = r_0/r$ is the extension ratio of a membrane element relative to the unstressed shape, B is the bending modulus and k_0 is the unstressed curvature. The unstressed shape is assumed to be a sphere (Secomb *et al.* 1986). The bending moments are assumed to be isotropic (Evans & Skalak 1980), and are given by

$$m_s = m_\phi = B(k_s + k_\phi - k_0) \tag{2.3}$$

The curvatures k_ϕ and k_s are given by

$$k_\phi = \frac{\sin\theta}{r}, \quad k_s = \frac{\mathrm{d}\theta}{\mathrm{d}s}. \tag{2.4}$$

The external forces are the pressure difference $p(s)$ between the external and internal fluids and viscous stress $\tau(s)$ due to the external fluid. The equations for equilibrium of normal stress, tangential stress and bending moments in the membrane are (Secomb *et al.* 1986; Secomb 1987):

$$\frac{1}{r}\frac{\mathrm{d}}{\mathrm{d}s}(rq_s) = p + k_s t_s + k_\phi t_\phi, \tag{2.4}$$

$$\frac{1}{r}\frac{\mathrm{d}}{\mathrm{d}s}(rt_s) = \frac{t_\phi \cos\theta}{r} - k_s q_s - \tau, \tag{2.5}$$

$$\frac{1}{r}\frac{\mathrm{d}}{\mathrm{d}s}(rm_s) = \frac{m_\phi \cos\theta}{r} + q_s. \tag{2.6}$$

2.2. *Lubrication theory*

The flow of the suspending fluid can be modelled using Stokes equations in cylindrical coordinates (σ, ϕ, z). The further approximations of lubrication theory can be made since the angle between the membrane and vessel wall is small over most of the length of the cell. At the front and rear of the cell, the gap between the cell and the wall widens, and the angle is no longer small. However, lubrication theory can still be used without introducing significant errors, since it is found that pressure gradients in these regions are small compared with their values in the narrow-gap region. Further justification for this approximation is given in §4.1. The momentum equation in the axial direction is then

$$\frac{\mu}{\sigma}\frac{\partial}{\partial\sigma}\left(\sigma\frac{\partial u}{\partial\sigma}\right) = \frac{\mathrm{d}p}{\mathrm{d}z}, \tag{2.7}$$

where u is the axial component of velocity and the pressure p is a function of z only. We fix the axes in the cell so that the boundary conditions are $u = 0$ on the membrane surface $\sigma = r(z)$ and $u = u_0$ at the vessel wall $\sigma = a$, where $r(z)$ defines the membrane surface, u_0 is the cell velocity and a the vessel radius (figure 1*b*). Equation (2.7) can then be integrated and the pressure gradient is given by (Secomb *et al.* 1986)

$$\frac{\mathrm{d}p}{\mathrm{d}z} = g(r) = \frac{16\mu}{a^2-r^2}\left[u_0\left[\tfrac{1}{2}a^2+\frac{a^2-r^2}{4\log(r/a)}\right]-aq_0\right]\left[a^2+r^2+\frac{a^2-r^2}{\log(r/a)}\right]^{-1}, \tag{2.8}$$

where

$$q_0 = \int_r^a u(\sigma, z)\frac{\sigma}{a}\mathrm{d}\sigma \tag{2.9}$$

is known as the leakback, the volume flow per unit vessel circumference relative to the cell, and is independent of z. The shear stress on the cell is

$$\tau(r) = \tfrac{1}{4}g(r)\left[\frac{a^2-r^2}{r\log(r/a)}+2r\right]-\frac{\mu u_0}{r\log(r/a)}. \tag{2.10}$$

If the gap width is assumed small compared with the vessel radius, then a two-dimensional approximation to (2.8) may be deduced by setting $r = a-h$ where $h \ll a$. This form is standard in lubrication theory, and is derived more simply starting with the two-dimensional approximation to (2.7):

$$\mu\frac{\mathrm{d}^2u}{\mathrm{d}y^2} = \frac{\mathrm{d}p}{\mathrm{d}z}, \tag{2.11}$$

where $y = a-\sigma$, $u(y)$ is the axial velocity and $p(z)$ is the pressure. The boundary conditions are $u = 0$ when $y = h$, and $u = u_0$ when $y = 0$. The pressure gradient can then be written in terms of the constant leakback q_0 and the gap width:

$$\frac{\mathrm{d}p}{\mathrm{d}z} = g(h) = -\frac{12\mu q_0}{h^3}+\frac{6\mu u_0}{h^2}$$

where

$$q_0 = \int_0^h u\,\mathrm{d}y. \tag{2.12}$$

The shear stresses acting on the cell membrane and the tube wall are, respectively,

$$\tau(h) = 6\mu q_0 h^{-2}-2\mu u_0 h^{-1}, \quad \tau_w(h) = 6\mu q_0 h^{-2}-4\mu u_0 h^{-1}. \tag{2.13}$$

This two-dimensional form is simpler than the axisymmetric form, and equivalent to it when the gap is very narrow. However, it has been shown that the axisymmetric form yields more accurate results if the gap is not very narrow relative to the tube radius (Secomb *et al.* 1986). Both forms are used below.

2.3. *System of equations*

The complete problem is specified by combining the equations of axisymmetric lubrication theory, (2.8) and (2.10), with those of membrane equilibrium, (2.4), (2.5) and (2.6). A system of first-order ordinary differential equations is obtained with arclength s as the independent variable:

$$\frac{\mathrm{d}r}{\mathrm{d}s} = \cos\theta, \tag{2.14}$$

$$\frac{\mathrm{d}\theta}{\mathrm{d}s} = k_s, \tag{2.15}$$

$$\frac{\mathrm{d}k_s}{\mathrm{d}s} = \frac{\sin\theta\cos\theta}{r^2} - \frac{\cos\theta}{r}k_s + \frac{q_s}{B}, \tag{2.16}$$

$$\frac{\mathrm{d}q_s}{\mathrm{d}s} = p + k_s t_s + \frac{\sin\theta}{r}\left[t_s - \kappa(\lambda_s^2 - \lambda_s^{-2}) + B\left(k_s - \frac{\sin\theta}{r}\right)\left(k_s + \frac{\sin\theta}{r} - k_0\right)\right] - \frac{q_s\cos\theta}{r}, \tag{2.17}$$

$$\frac{\mathrm{d}p}{\mathrm{d}s} = g(r)\sin\theta, \tag{2.18}$$

$$\frac{\mathrm{d}t_s}{\mathrm{d}s} = -\frac{\cos\theta}{r}\left[\kappa(\lambda_s^2 - \lambda_s^{-2}) - B\left(k_s - \frac{\sin\theta}{r}\right)\left(k_s + \frac{\sin\theta}{r} - k_0\right)\right] - k_s q_s - \tau(r). \tag{2.19}$$

The boundary conditions are that r and $\sin\theta$ vanish on the axis and that the surface area and volume are prescribed. The classical assumptions of lubrication theory suggest that $g(r)\sin\theta$ could be replaced by $g(r)$, and $\tau(r)$ by $\tau(r)\sin\theta$ in (2.18) and (2.19) respectively. However, analysis of Stokes flow in a corner (§4.1) shows that (2.18) and (2.19) give better results when θ is not small.

In the high-velocity limit, the fluid stresses are balanced by isotropic tensions generated in the cell membrane. Then both shear and bending resistance are neglected and the above system of equations reduces to the following four equations:

$$\frac{\mathrm{d}r}{\mathrm{d}s} = \cos\theta, \tag{2.20}$$

$$\frac{\mathrm{d}\theta}{\mathrm{d}s} = -\frac{p}{t_s} - \frac{\sin\theta}{r}, \tag{2.21}$$

$$\frac{\mathrm{d}p}{\mathrm{d}s} = g(r)\sin\theta, \tag{2.22}$$

$$\frac{\mathrm{d}t_s}{\mathrm{d}s} = -\tau(r). \tag{2.23}$$

In this case the solutions are independent of u_0, the cell velocity. This limit will be considered in detail in §§3 and 4.

3. Solutions for near-critical cell shapes

3.1. *Rigid particles*

In a vessel of near-minimal diameter, the red cell necessarily assumes a shape close to the critical shape already discussed. Secomb & Gross (1983) gave an approximate analysis of this case, assuming that the cell behaves as a rigid body with the critical shape. This analysis used two-dimensional lubrication theory, with a quadratic approximation to the gap width $h(z)$. Özkaya & Skalak (1983) and Özkaya (1986) showed that closed-form solutions could be obtained even if this quadratic approximation was not used. For very elongated cell shapes, the two approaches yield very similar results, but the approach of Özkaya & Skalak (1983) is more accurate for less elongated shapes.

Here we summarize the analysis of Özkaya & Skalak (1983), and extend it slightly to consider particles with spheroidal end regions of different lengths. We consider a body with a central cylindrical section of length βa and radius λa, and hemispheroidal ends of length αa and γa (figure 2). The pressure drop along the cell may be obtained by integrating (2.9):

$$\Delta p = \frac{6\mu u_0}{a}\left\{(\alpha+\gamma)(I_2 - CI_3) + \beta\left[\frac{1}{(1-\lambda)^2} - \frac{C}{(1-\lambda)^3}\right]\right\}, \tag{3.1}$$

where

$$I_n = \int_0^{\pi/2} \frac{\sin\theta}{(1-\lambda\sin\theta)^n}\,\mathrm{d}\theta \quad \text{for} \quad n = 1, 2, 3, \tag{3.2}$$

and $C = 2q_0/au_0$. To evaluate q_0 for rigid particles, we use the zero-drag condition, applied to a cylindrical region of radius a and the length of the cell. In this case,

$$\pi a^2 \Delta p + F = 0, \tag{3.3}$$

where F is obtained by integrating τ_w (equation (2.13)) over the tube surface bounding the region, yielding

$$F = 2\pi a\mu u_0\left[(\alpha+\gamma)(3CI_2 - 4I_1) + \beta\left(\frac{3C}{(1-\lambda)^2} - \frac{4}{1-\lambda}\right)\right]. \tag{3.4}$$

Equation (3.2) can be integrated (Gradshteyn & Ryzhik 1980):

$$I_1 = \frac{2\lambda^* - \pi/2}{\lambda}, \quad I_2 = \frac{1+2\lambda\lambda^*}{1-\lambda^2}, \quad I_3 = \frac{1+\lambda^2/2+3\lambda\lambda^*}{(1-\lambda^2)^2}, \tag{3.5}$$

where

$$\lambda^* = \frac{1}{(1-\lambda^2)^{\frac{1}{2}}}\left[\tan^{-1}\frac{1-\lambda}{(1-\lambda^2)^{\frac{1}{2}}} + \tan^{-1}\frac{\lambda}{(1-\lambda^2)^{\frac{1}{2}}}\right]. \tag{3.6}$$

For given values of α, γ, β and λ, Δp and q_0 can be computed. Özkaya (1986) gives a more detailed analysis covering a variety of particle geometries. We use the above results in §5.

3.2. *Flexible particles: outer solutions*

When the tube radius a is only slightly larger than the critical radius r_c for a flexible particle, the constraints of constant surface area and volume imply that the cell shape must be close to the near-critical shape. In this section, we show that the governing equations for flexible particles permit solutions for membrane shape with cylindrical and hemispherical 'outer' regions, as indicated in figure 3. Similar solutions were derived by Secomb *et al.* (1986) for cells with concave rear regions.

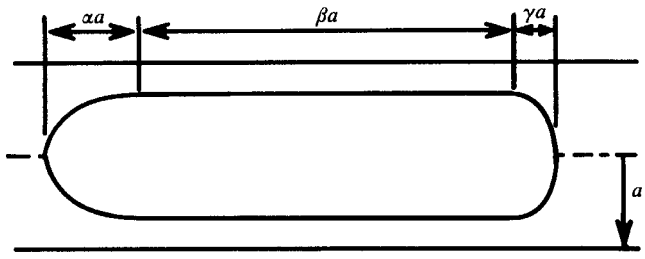

FIGURE 2. Assumed geometry of a rigid particle flowing through a tube of radius a. The particle consists of a cylindrical part of length βa and hemispheroidal ends of length αa and γa.

One solution to (2.20)–(2.23) corresponds to a cylindrical membrane (region III):

$$\theta = \tfrac{1}{2}\pi, \quad r = r_c, \quad p = g(r_c)(s-s_c) - \frac{t_{si}}{r_c}, \quad t_s = -r_c g(r_c)(s-s_c) + t_{si}, \tag{3.7}$$

where r_c is the cell radius, and t_{si} is a constant such that $t_s = t_{si}$ at $s = s_c = \frac{1}{2}\pi r_c$. A second approximate solution to (2.20)–(2.23) is obtained by noting that, according to (2.12) and (2.13), both the pressure and tension are constants (to leading order) when h is no longer small. The outer solution in region I is then

$$\theta = s/r_c, \quad r = r_c \sin\theta, \quad p = -p_i, \quad t_s = t_{si}, \tag{3.8}$$

where $0 \leqslant s \leqslant \frac{1}{2}\pi r_c$, $r_c = 2t_{si}/p_i$, p_i is the internal pressure of the cell and the external pressure in this region is set to zero. Similarly, the solution in region V is

$$\theta = (s-s_t)/r_c + \pi, \quad r = r_c \sin\theta, \quad p = p_0 - p_i, \quad t_s = t_{so} \tag{3.9}$$

where $\frac{1}{2}\pi r_c + l_c \leqslant s \leqslant s_t = \pi r_c + l_c$, $t_{so} = \frac{1}{2}(p_i - p_0) r_c$ and p_0 is the external pressure in this region.

There is an abrupt change in membrane curvature and hence in pressure at the points near the front and rear of the cell where the outer solutions meet. Therefore, the outer solutions must be matched through narrow transition regions (II and IV), to remove these discontinuities. These transition regions are analysed in §§3.3 and 4.2.

3.3. *Flexible particles: transition regions in the high-tension limit*

For sufficiently small tube diameters, the tension is large in all parts of the cell membrane. In this case, we suppose that the non-dimensional gap width $\epsilon = 1 - r_c/a$ is small and use the two-dimensional form of lubrication theory, (2.12) and (2.13), making the further assumption that variations of θ from $\frac{1}{2}\pi$ are small. The following set of scalings is introduced:

$$h = \epsilon r_c H, \quad q_0 = \tfrac{1}{2}\epsilon r_c u_0 Q_0, \quad s = r_c \delta_1 S, \quad p = \frac{\mu u_0}{r_c}\delta_2 P, \quad t_s = \mu u_0 \delta_3 T, \quad \theta = \tfrac{1}{2}\pi + \delta_4 \theta', \tag{3.10}$$

where S, the independent variable, and H, Q_0, P, T, θ' are all of order one as $\epsilon \to 0$. If these are substituted into (2.20)–(2.23), and powers of δ_i and ϵ are equated, then it is found that

$$(\delta_1, \delta_2, \delta_3) = (\epsilon\delta_4^{-1}, \epsilon^{-1}\delta_4^{-1}, \delta_4^{-3}). \tag{3.11}$$

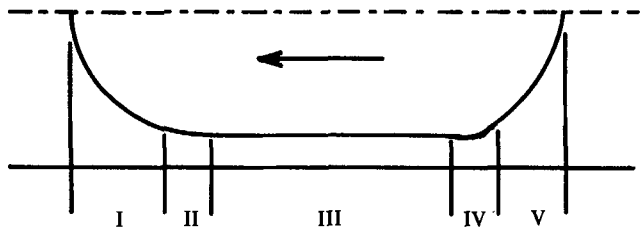

FIGURE 3. Membrane regions used in asymptotic analysis: two 'outer' hemispherical regions (I and V), an 'outer' cylindrical region (III) and two 'inner' transition regions (II and IV).

For matching with the outer solutions (regions I, III and V), we require that the curvature is $O(1)$, i.e. $\delta_4/\delta_1 = O(1)$. So

$$(\delta_1, \delta_2, \delta_3, \delta_4) = (\epsilon^{\frac{1}{2}}, \epsilon^{-\frac{3}{2}}, \epsilon^{-\frac{3}{2}}, \epsilon^{\frac{1}{2}}). \tag{3.12}$$

These scalings imply that the tension is high and approximately constant in the transition regions, and are consistent with those obtained by Secomb *et al.* (1986) for the front transition region.

The following system of equations is obtained at leading order in both transition regions:

$$\frac{\mathrm{d}H}{\mathrm{d}S} = \theta', \tag{3.13}$$

$$\frac{\mathrm{d}\theta'}{\mathrm{d}S} = -\frac{P}{T} - 1, \tag{3.14}$$

$$\frac{\mathrm{d}P}{\mathrm{d}S} = 6(H^{-2} - Q_0 H^{-3}), \tag{3.15}$$

$$\frac{\mathrm{d}T}{\mathrm{d}S} = 0. \tag{3.16}$$

For matching with the cylindrical region III, in which $H = 1$, the above scalings imply that $\mathrm{d}P/\mathrm{d}S \to 0$ as $H \to 1$, and so $Q_0 = 1$ at leading order, i.e. $q_0 = \frac{1}{2}\epsilon r_c u_0$. The tension T is replaced by constants T_i, where $i = 1$ at the front, and $i = 2$ at the rear, and new independent variables are introduced:

$$\xi_i = T_i^{-\frac{1}{3}}(S - S_{\mathrm{m}i}). \tag{3.17}$$

It is convenient to set the origins of the inner coordinates ξ_i at $S = S_{\mathrm{m}i}$, where $H(S_{\mathrm{m}i}) = \frac{3}{2}$. With this choice, $\tau = 0$ at the origins. Let $H(S) = f_i(\xi_i)$. Then

$$f_i''' = 6(f_i^{-3} - f_i^{-2}) \tag{3.18}$$

with boundary conditions

$$f_1' \to 0 \quad \text{as } \xi_1 \to \infty, \quad f_1(0) = \tfrac{3}{2}, \tag{3.19}$$

and

$$f_2' \to 0 \quad \text{as } \xi_2 \to -\infty, \quad f_2(0) = \tfrac{3}{2}. \tag{3.20}$$

Since only two boundary conditions are available, the solutions are not necessarily unique. Although (3.18) cannot be solved in closed form, differences between the front and rear transition regions can be shown by linearizing about the solution

$f_i = 1$ which applies in the cylindrical region. Setting $f_i = 1 + \delta\Phi_i$ where $\delta \ll 1$ and substituting into (3.18), we obtain at leading order

$$\Phi_i''' + 6\Phi_i = 0. \tag{3.21}$$

The general solution is

$$\Phi_i(\xi_i) = A_i e^{m_1\xi_i} + e^{-m_1\xi_i/2}\left[B_i \cos\left(\frac{m_1\sqrt{3}\xi_i}{2}\right) + C_i \sin\left(\frac{m_1\sqrt{3}\xi_i}{2}\right)\right], \tag{3.22}$$

where $m_1 = -6^{\frac{1}{3}}$, and A_i, B_i, C_i are to be determined by applying the boundary conditions.

At the front transition, (3.19) implies that $B_1 = C_1 = 0$, and so Φ_1 is uniquely determined (Secomb *et al.* 1986). The same holds for the nonlinear equation (3.18) and the function f_1 and its derivatives are obtained numerically (figure 4*a*). The transition from the hemispherical to the cylindrical region is smooth and monotonic.

At the rear transition,(3.20) implies only that $A_2 = 0$, and so there is one remaining degree of freedom in Φ_2 and f_2, which must be determined by matching with the rear transition region. An example of f_2 is shown in figure 4(*b*). In this case the solution at the rear has oscillatory modes which are not present at the front. The gap width (f) shows a local minimum before it widens in the rear region. This behaviour is characteristic of lubrication solutions with flexible membranes. The above theory for the transition regions is similar to that applied to the motion of long bubbles in capillary tubes (Bretherton 1961).

To match the transition solutions with the upstream and downstream solutions, we consider the pressure

$$P(\xi_i) = -T_i[1 + T_i^{-\frac{2}{3}} f_i''(\xi_i)]. \tag{3.23}$$

At the front, numerical integration of (3.18) shows that $f_1'' \to k_1 \approx 2.123$ as $\xi_1 \to -\infty$. Since $P \to -P_1$ as $\xi_1 \to -\infty$ and $P_1 = 2T_1$ to leading order, (3.23) implies that

$$T_1 = k_1^{\frac{3}{2}}. \tag{3.24}$$

The tension T_2 in the rear transition region can be determined by using (2.13) and (2.23):

$$T_2 = k_1^{\frac{3}{2}} - \epsilon^{\frac{1}{2}} l_c/r_c. \tag{3.25}$$

Now suppose $f_2'' \to k_2$ as $\xi_2 \to \infty$. Since $P \to P_0 - P_1$ as $\xi_2 \to \infty$ and $P_1 - P_0 = 2T_2$,

$$T_2 = k_2^{\frac{3}{2}}. \tag{3.26}$$

Then k_2 is determined by equating (3.25) and (3.26), and f_2 is uniquely determined. The pressure drop across the cell is given by

$$\Delta P = 2\epsilon^{\frac{1}{2}} l_c/r_c. \tag{3.27}$$

From (3.25), the assumption that the tension T_2 is high in the rear transition region will not be valid if ϵ reaches a value

$$\epsilon_c = \frac{k_1^3 r_c^2}{l_c^2}. \tag{3.28}$$

For cells with $V = 90\ \mu m^3$ and $A = 135\ \mu m^2$, $\epsilon_c \approx 0.129$. The corresponding vessel radius is $a_c \approx 1.61\ \mu m$. Note that for cells with higher sphericity indices, this estimate for ϵ_c may be inaccurate since ϵ_c is no longer small. For example, if $V = 109.6\ \mu m^3$ and $A = 135\ \mu m^2$, then $\epsilon_c \approx 0.456$.

As the vessel radius approaches a_c, the above asymptotic analysis has to be

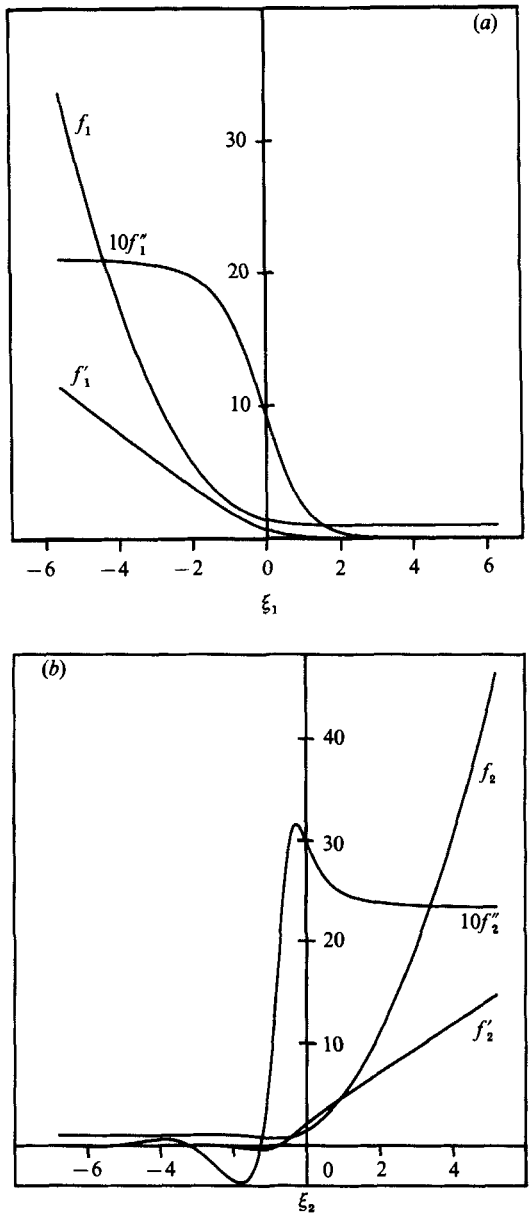

FIGURE 4. The functions f_1 and f_2 and their derivatives. (*a*) Front transition region (f_1). (*b*) Example of f_2 in rear transition region.

modified, since the tension at the rear transition region is no longer $O(\epsilon^{-\frac{3}{2}})$ and cannot be assumed to be approximately constant. This case is considered next.

4. Solution for less elongated cell shapes

4.1. *Validity of lubrication theory in a corner flow*

In the previous analysis, the use of lubrication theory uniformly over the cell length was justified on the basis that the angle between the membrane and the wall was

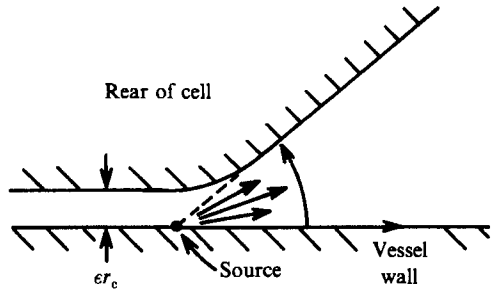

FIGURE 5. Geometry assumed for analysis of flow in a corner.

small in all regions where the gap width was not large. However, (3.14) suggests that the angle θ' may be $O(1)$ if the tension becomes sufficiently small in the rear transition, and so the applicability of lubrication theory should be examined. An indication of the accuracy of the lubrication theory approximation is obtained by a comparison with exact similarity solutions for the case of two-dimensional Stokes flow in a corner formed by one rigid plane sliding steadily over another (Batchelor 1967), with a point source at the intersection of the two planes (figure 5). The comparison is made by evaluating the non-dimensionalised pressure gradient p_g and the shear stress τ on the inclined wall. The rear of the cell is approximated by two straight line segments as shown in figure 5.

The solution to the Stokes flow problem is determined by introducing a stream function ψ, which satisfies the biharmonic equation:

$$\nabla^4 \psi = 0. \tag{4.1}$$

In this case, $\psi = \psi_c + \psi_s$ where the subscript c refers to the corner flow driven by the moving boundary (Batchelor 1967, p. 225) and s to the source flow. Similarity solutions are available in the form

$$\psi_c(r,\theta) = rf(\theta), \quad \psi_s(r,\theta) = g(\theta), \tag{4.2}$$

where r and θ are the usual polar coordinates, and f and g satisfy

$$f'''' + 2f'' + f = 0, \quad f(0) = f(\theta_0) = f'(\theta_0) = 0, \quad f'(0) = u_0, \tag{4.3}$$

$$g'''' + 4g'' = 0, \quad g'(0) = g'(\theta_0) = 0, \tag{4.4}$$

where θ_0 is the angle between the two planes. The wall shear stress and pressure gradient are then given by

$$\tau = \frac{1}{R^2}\frac{\partial^2 \psi}{\partial \theta^2}\bigg|_{\theta=\theta_0} = \frac{f''(\theta_0)}{R} + \frac{g''(\theta_0)}{R^2} \tag{4.5}$$

and

$$p_g = \frac{1}{R}\frac{\partial}{\partial \theta}\nabla^2 \psi\bigg|_{\theta=\theta_0} = \frac{f'''(\theta_0)}{R^2} + \frac{g'''(\theta_0)}{R^3} \tag{4.6}$$

where R is the non-dimensional distance from the intersection of the two planes.

The resulting estimates of shear stress (τ_0 for Stokes flow solution, τ_1 for lubrication theory) can be written

$$\tau_i = \frac{\epsilon G_i(\theta_0)}{\theta_0^2 R^2} - \frac{F_i(\theta_0)}{\theta_0 R} \quad \text{for} \quad i = 0, 1. \tag{4.7}$$

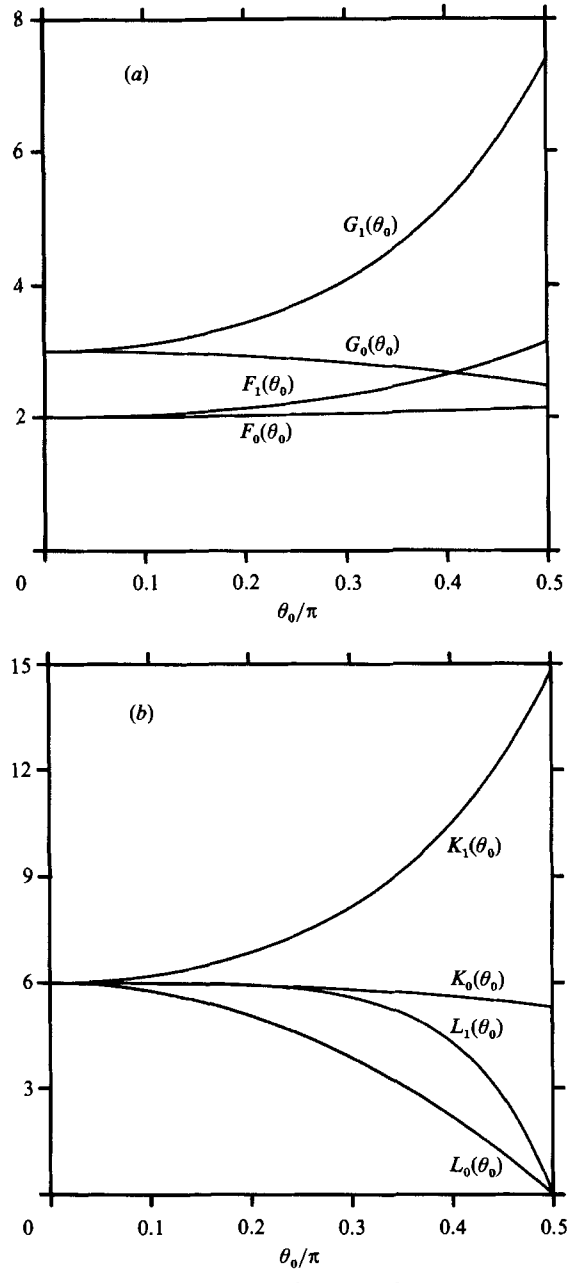

FIGURE 6. Comparison of results of lubrication theory and similarity solution for Stokes flow in a corner. (*a*) $G_i(\theta_0)$ and $F_i(\theta_0)$. (*b*) $K_i(\theta_0)$ and $L_i(\theta_0)$.

F_i and G_i are defined so as to approach finite non-zero values when θ_0 is small, and

$$G_0(\theta_0) = \frac{\theta_0^2 \sin\theta_0}{\sin\theta_0 - \theta_0\cos\theta_0}, \quad G_1(\theta_0) = \frac{3\theta_0^2}{\sin^2\theta_0}, \tag{4.8}$$

$$F_0(\theta_0) = \frac{2\theta_0(\sin\theta_0 - \theta_0\cos\theta_0)}{\theta_0^2 - \sin^2\theta_0}, \quad F_1(\theta_0) = \frac{2\theta_0}{\sin\theta_0}. \tag{4.9}$$

Similarly, the estimates of pressure gradient are

$$p_{g_i} = \frac{K_i(\theta_0)}{\theta_0^2 R^2} - \frac{\epsilon L_i(\theta_0)}{\theta_0^3 R^3}, \tag{4.10}$$

where

$$K_0(\theta_0) = \frac{2\theta_0^3 \sin\theta_0}{\theta_0^2 - \sin^2\theta_0}, \quad K_1(\theta_0) = \frac{6\theta_0^2}{\sin^2\theta_0}, \tag{4.11}$$

$$L_0(\theta_0) = \frac{2\theta_0^3 \cos\theta_0}{\sin\theta_0 - \theta_0\cos\theta_0}, \quad L_1(\theta_0) = \frac{6\theta_0^3\cos\theta_0}{\sin^3\theta_0}. \tag{4.12}$$

Figure 6 shows that the two methods yield very close results when θ_0 is small. Even for values of θ_0 as large as 45°, the results of the two methods differ by at most 20%, suggesting that lubrication theory as formulated in §2.2 can yield useful results for finite angles.

4.2. *Intermediate tension at the rear*

As the vessel radius increases, the tension in the rear transition region decreases according to (3.25). Eventually, large curvatures occur in the transition region, from (2.21), and it is then necessary to reconsider the scalings introduced in (3.10). Equation (3.11) still applies, but the scalings (3.12) no longer hold, since the curvature is large ($\delta_4/\delta_1 \gg 1$). From (3.11), $\delta_1 \ll \epsilon^{\frac{1}{2}}$, $\delta_2 \ll \epsilon^{-\frac{3}{2}}$, $\delta_3 \ll \epsilon^{-\frac{3}{2}}$ and $\delta_4 \gg \epsilon^{\frac{1}{2}}$ in this case. In particular, the tension in the transition is $o(\mu u_0 \epsilon^{-\frac{3}{2}})$. We leave the scalings undetermined, but assume that changes in membrane angle within the transition region are small, i.e. $\delta_4 \ll 1$.

With these scalings, the following system is obtained at leading order:

$$\frac{dH}{dS} = \theta', \quad \frac{d\theta'}{dS} = -\frac{P}{T}, \quad \frac{dP}{dS} = 6(H^{-2} - H^{-3}), \quad \frac{dT}{dS} = 0. \tag{4.13}$$

As in §3.3, we introduce a scaled coordinate $\xi = T^{-\frac{1}{3}}(S - S_m)$, let $H(S) = f(\xi)$, and obtain an equation analogous to (3.18):

$$f''' = 6(f^{-3} - f^{-2})$$

with

$$f(0) = \tfrac{3}{2}, \quad f' \to 0 \quad \text{as} \quad \xi \to -\infty \quad \text{and} \quad f'' \to 0 \quad \text{as} \quad \xi \to \infty. \tag{4.14}$$

The additional condition $f'' \to 0$ as $\xi \to \infty$ is imposed (cf. (3.20)) since the curvature is large in the transition region, but is $O(1)$ in the outer region (V).

For large ξ, (4.14) can be approximated by the simpler equation $f''' = -6f^{-2}$, which has two possible asymptotic solutions as $\xi \to \infty$, of the form (Bender & Orszag 1978, pp. 156–158):

$$f_{a1} \approx \alpha\xi^2 + \beta\xi + \gamma + \sum_{k=1}^{\infty} \delta_k \xi^{-k}, \tag{4.15}$$

and

$$f_{a2} \approx \xi(18\log\xi)^{\frac{1}{3}}\left(1 + \frac{A}{\log\xi} + \sum_{k=1}^{\infty} B_k(\log\xi)^{-(k+1)}\right), \tag{4.16}$$

where α, β and γ are arbitrary, and δ_k contains terms of order α^{-1}. The solution f_{a1} corresponds to the result obtained in the high-tension limit (§3.3), and from (3.26), the tension in the rear transition is $T_2 = (2\alpha)^{\frac{3}{2}}$, since $f''_{a1} \to 2\alpha$ as $\xi \to \infty$. As the gap width ϵ approaches the value ϵ_c given by (3.28), the tension decreases, α approaches zero and f_{a1} becomes singular. The asymptotic solution for the intermediate-tension case considered here is f_{a2}, which satisfies the condition $f''_{a2} \to 0$ as $\xi \to \infty$. The corresponding unique solution to (4.14) was obtained by numerical integration over

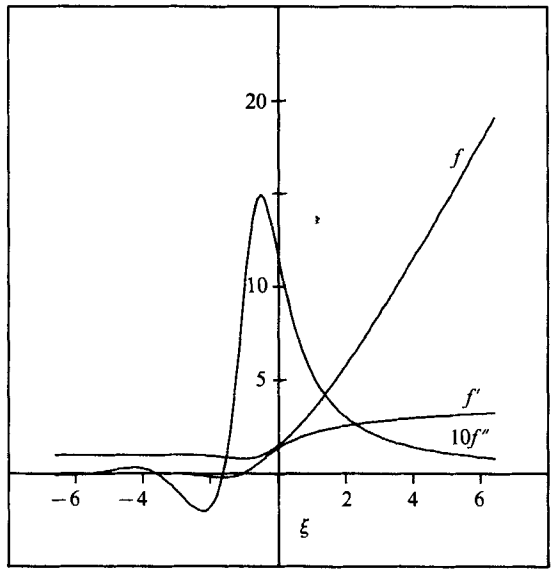

FIGURE 7. The function f and its derivatives for the intermediate-tension case.

a finite range of ξ and matching to (4.16). The function f and its derivatives are shown in figure 7. We conclude that when the tension becomes smaller than $O(\mu u_0 \epsilon^{-\frac{3}{2}})$ in the rear transition region, high curvatures are generated locally. Beyond the high-curvature region, the angle $(\theta - \frac{1}{2}\pi)$ between the membrane and the wall grows as $(\log \xi)^{\frac{1}{3}}$, rather than linearly with ξ as in the high-tension case.

In general, the angle $\theta - \frac{1}{2}\pi$ remains small in the transition region. However, if the tension is decreased sufficiently, this angle eventually attains $O(1)$ values at its matching with the outer solution in region V. In this case, $\delta_4 \theta' = O(1)$ when $\delta_1(S - S_m) = O(1)$. From (4.13) and (4.16) we find that $\theta' \approx (18 \log \xi / T)^{\frac{1}{3}}$ for large ξ. Hence

$$\delta_4 (\log (1/\delta_1))^{\frac{1}{3}} = O(1). \tag{4.17}$$

Using (3.11), we deduce that this case occurs for the following scalings:

$$(\delta_1, \delta_2, \delta_3, \delta_4) = (\epsilon |\log \epsilon|^{\frac{1}{3}}, \epsilon^{-1} |\log \epsilon|^{\frac{1}{3}}, |\log \epsilon|, |\log \epsilon|^{-\frac{1}{3}}), \tag{4.18}$$

which is consistent with the original assumption that $\epsilon^{\frac{1}{2}} \ll \delta_4 \ll 1$. Thus, when the tension drops to $O(\mu u_0 |\log \epsilon|)$ in the rear transition region, the angle between the membrane and the wall attains an $O(1)$ value $(\theta_m - \frac{1}{2}\pi)$ at the matching with the outer solution, and θ_m is given asymptotically by

$$\theta_m \approx \tfrac{1}{2}\pi + (18 \mu u_0 |\log \epsilon| / t_s)^{\frac{1}{3}}, \tag{4.19}$$

where t_s is the tension in the transition region.

The findings of this section are qualitatively consistent with the solutions postulated by Secomb & Gross (1983), in which the membrane tension reaches zero at the rear of the lubrication layer and the membrane angle has a discontinuity. This physically unrealistic behaviour is a consequence of the neglect of bending resistance in the membrane. The effects of bending resistance are considered in the next section.

5. Numerical solutions for cell shape

The boundary-value problems stated in §2.3 can be solved numerically. First, a new independent variable χ is introduced, such that

$$2\pi R_0 \sin\chi R_0 \,\mathrm{d}\chi = 2\pi r \,\mathrm{d}s, \tag{5.1}$$

where R_0 is the radius of a sphere with the same surface area as the red cell. This procedure fixes the computational domain, $0 \leqslant \chi \leqslant \pi$. Since the differential equations are singular on the axis, at $\chi = 0$ and π, they are integrated over a slightly reduced domain, $\delta \leqslant \chi \leqslant \pi - \delta$, with $\delta = \pi/m$ ($m \geqslant 30$), and matched to segments of circles at either end. The above system is stiff and ill-conditioned, and was solved using multiple-shooting and finite-difference methods.

Cell shapes, pressure and tension distributions computed using the isotropic tension model (equations (2.20)–(2.23)) are shown in figure 8, for vessel radii of 1.451 μm and 1.572 μm. The numerical results are consistent with predictions made in previous sections. The isotropic tension does not vary much in the entrance region and decreases linearly in the cylindrical region until it reaches a minimum in the rear transition region. The pressure initially rises rapidly, then linearly in the cylindrical region, and oscillates at the rear where the cell shows an outwards bulge. As the vessel radius increases, the rear end becomes less convex and eventually flat. Also, the amplitude of the pressure swing at the rear diminishes and the pressure variation becomes monotonic as the tension in the rear transition approaches zero. Further cell shapes are shown in figure 9 for cells with the same surface area ($A = 135\ \mu\mathrm{m}^2$) but different volumes.

Cell shapes are also computed using the model including shear and bending resistance (equations (2.14)–(2.19)). These are shown in figure 10 for a range of vessel radii. The cell velocity u_0 is chosen to be 0.01 cm/s, $\mu = 1$ cP, $\kappa = 0.0042$ dyn/cm and $B = 1.8 \times 10^{-12}$ dyn cm. These computed shapes demonstrate the effect of bending and shear. As the vessel radius increases and the tension at the rear of the cylindrical region decreases, the rear becomes less convex, then flat and finally concave. The transition from convex to concave shapes is also a function of cell velocity. At higher velocities, it occurs at slightly larger vessel radii.

Two rheological parameters with physiological significance are the reduction of haematocrit due to the Fahraeus effect, and the apparent viscosity. By conservation of mass

$$\frac{H_\mathrm{T}}{H_\mathrm{D}} = \frac{\bar{u}}{u_0} = 1 - \frac{2q_0}{au_0}, \tag{5.2}$$

where H_T is the tube haematocrit, H_D the discharge haematocrit, and $\bar{u}$ the mean bulk velocity. The fact that H_T is less than H_D in general is known as the Fahraeus effect. We neglect cell-to-cell interactions, so that the apparent viscosity μ_app, depends linearly on the tube haematocrit

$$\mu_\mathrm{app} = \mu(1 + K_\mathrm{T} H_\mathrm{T}), \tag{5.3}$$

where K_T is the apparent intrinsic viscosity. Assuming that the pressure drop between cells is given by Poiseuille's law, we obtain

$$K_\mathrm{T} = \frac{\pi a^2}{V}\left[\frac{\Delta p a^2}{8\mu(u_0 - 2q_0/a)} - l\right], \tag{5.4}$$

where Δp is the pressure drop across the cell and l its length. The above expression

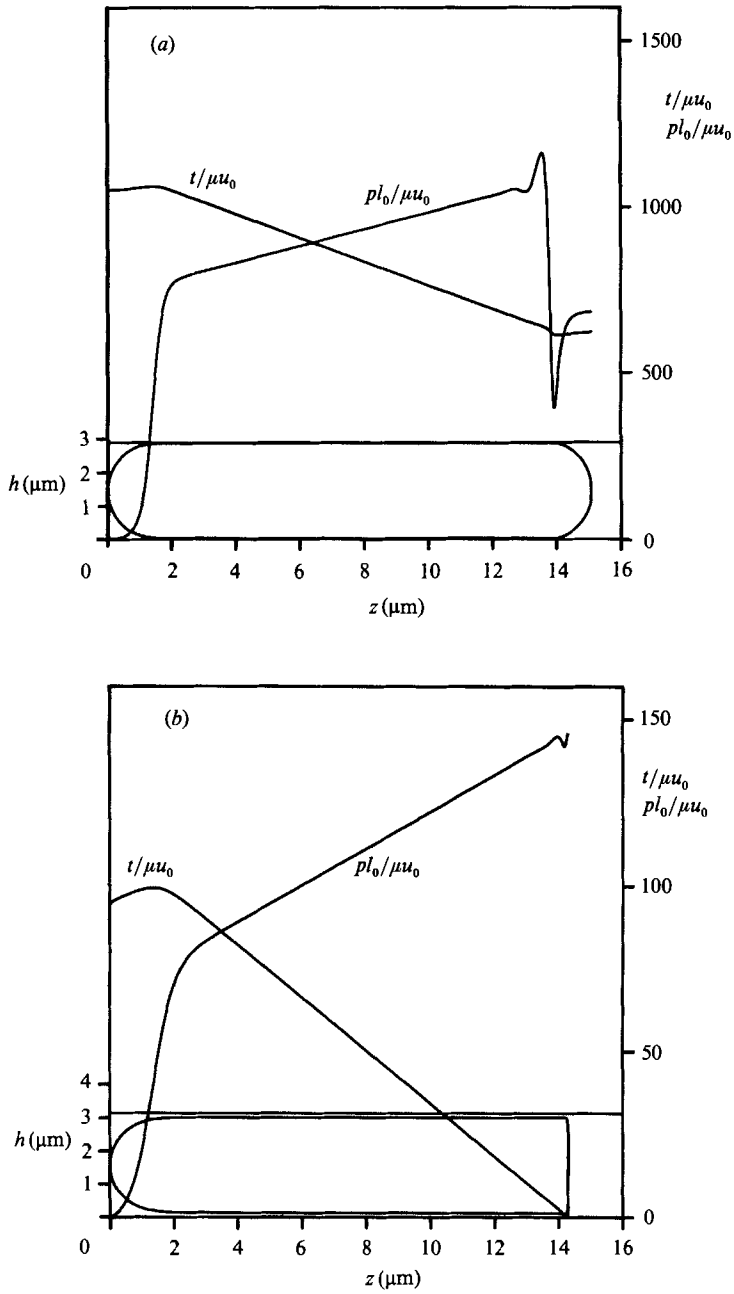

FIGURE 8. Numerical computed cell shapes and variations of pressure and isotropic tension for flexible particles with volume 90 μm³ and surface area 135 μm². (*a*) $a = 1.451$ μm, (*b*) $a = 1.572$ μm. Pressure and tension non-dimensionalized as shown, with $l_0 = 1$ μm.

for K_T is valid if the spacing between cells is of the order of one vessel radius or more (Secomb *et al.* 1986).

Values of K_T and Fahraeus effect as functions of vessel radius are shown in figure 11, computed using the rigid-particle approach of §3.1, the asymptotic approach of §§3.2 and 3.3, and the numerical solutions of both the isotropic and bending and

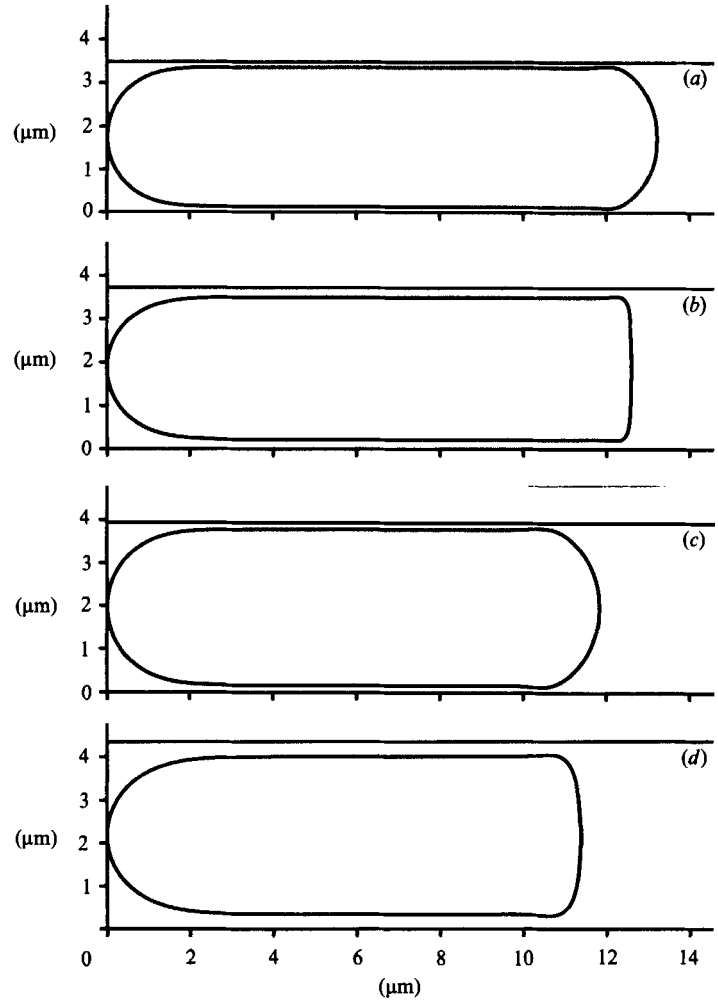

FIGURE 9. Computed shapes for cells with larger volumes. (*a*) $V = 100.2\ \mu m^3$, $a = 1.743\ \mu m$; (*b*) $V = 100.2\ \mu m^3$, $a = 1.863\ \mu m$; (*c*) $V = 109.6\ \mu m^3$, $a = 1.97\ \mu m$; (*d*) $V = 109.6\ \mu m^3$, $a = 2.175\ \mu m$.

shear models. Also included for comparison are results for larger vessel radii in which cells have concave rears (Secomb & Gross 1983).

The results obtained assuming a rigid particle with the critical shape agree well with the numerical results for a flexible particle. This is perhaps surprising, since the rigid-particle model neglects the bulging out at the rear which occurs with flexible particles, and the pressure fields around the particles are very sensitive to such differences in shape. For example, the rigid-particle model predicts a negative pressure gradient in the cylindrical region for a particle of critical shape in a vessel with a radius of 1.45 μm, as $C > 1-\lambda$ in (3.1). In contrast, the numerical solution (figure 8) shows a positive pressure gradient. The asymptotic results underestimate K_T, because only the pressure drop over the length of the cylindrical region is included at leading order. The estimates of K_T obtained from the bending and shear model are higher than those obtained from the model of Secomb & Gross (1983). Inclusion of shear and bending resistance makes the cell less deformable, resulting in narrower lubrication layers.

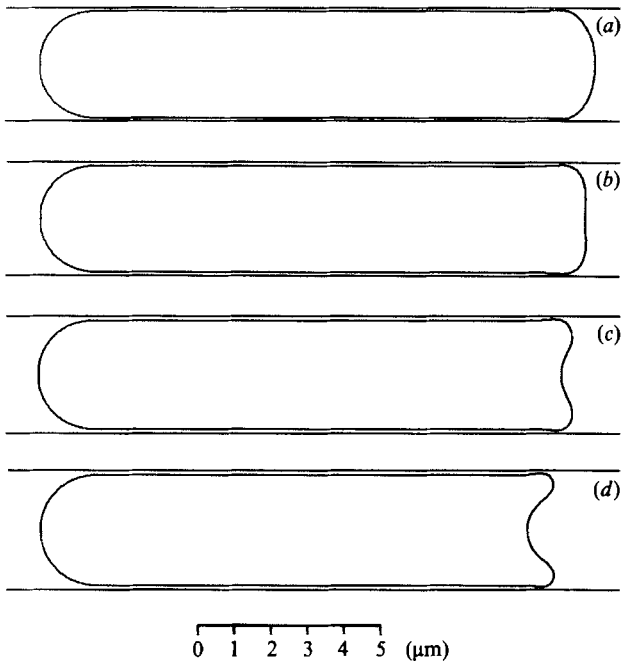

FIGURE 10. Numerically computed cell shapes including bending and shear resistance, with $V = 90\ \mu m^3$, $A = 135\ \mu m^2$. (*a*) $a = 1.5\ \mu m$, (*b*) $a = 1.52\ \mu m$, (*c*) $a = 1.55\ \mu m$, (*d*) $a = 1.6\ \mu m$.

6. Discussion and conclusions

The deformability of red blood cells allows them to traverse pathways such as capillaries with remarkable ease, even when the dimensions of these pathways are smaller than the radius of an unstressed red cell. However, in extremely narrow pathways such as may occur in bone marrow, spleen, and partially collapsed or occluded capillaries of other tissues, the red cell approaches the limits of its deformability. Although these pathways may have more complex geometries than the case considered here, they share the feature that the cell acquires a rigidity that it does not otherwise exhibit as the limitation of fixed surface area is reached. The problem considered here represents a prototype and starting point for analysing this phenomenon.

One significant finding is that the range of radii in which near-critical shapes occur is quite small. The minimal radius, in the case of human red cells, is 1.42 μm. For radii up to about 1.55 μm, the overall shape consists of a cylinder with two hemispherical ends. Further increases in the radius lead to a flattening of the rear of the cell, which is flat when the radius is 1.572 μm, according to the numerical calculations in the high-velocity limit. (The more approximate asymptotic theory of §3.3 predicts that this occurs at a radius of 1.61 μm.) These results are consistent with those obtained using the bending and shear model. As shown in figure 10, the shape of the cell is convex up to a radius of 1.52 μm at a cell velocity of 0.01 cm/s. The radius at which this transition in shape occurs increases with cell velocity, and the isotropic tension model gives the high-velocity limit.

The asymptotic analysis of the isotropic tension model provides insight into the variation of the cell from its critical shape as the vessel radius increases from the

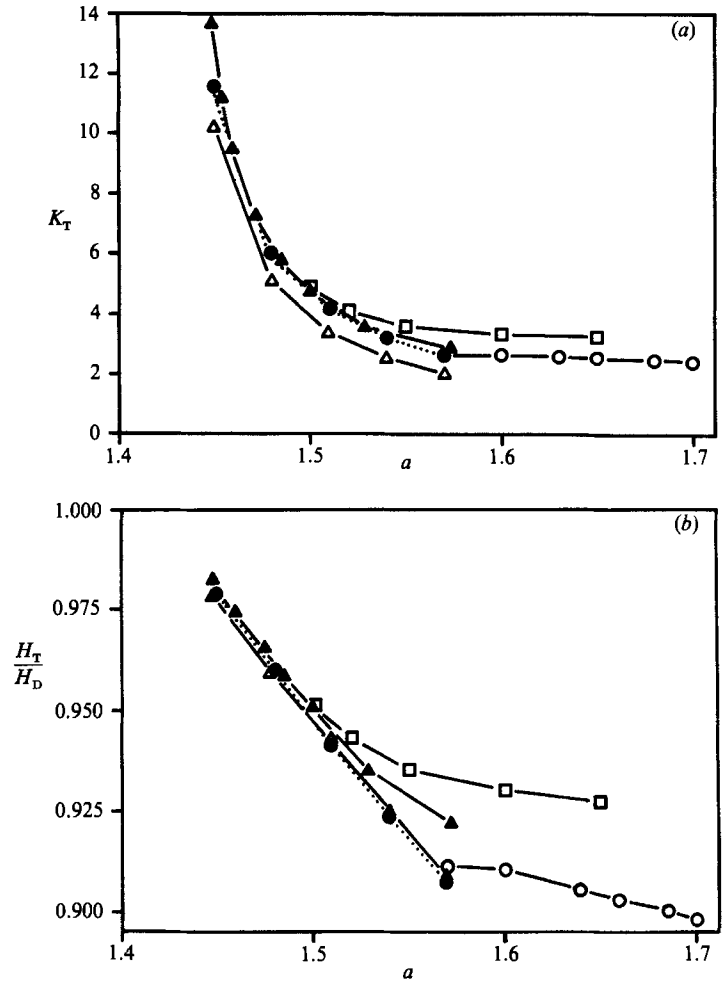

FIGURE 11. Computed rheological parameters for red cells with $V = 90\ \mu m^3$ and $A = 135\ \mu m^2$. ●, rigid-particle model; △, asymptotic results for flexible particles; □, numerical results for flexible particles with bending and shear resistance; ▲, numerical results for flexible particles using the isotropic tension model; ○, results of Secomb & Gross (1983) for flexible particles with concave rears. (*a*) Variation of apparent intrinsic viscosity K_T with vessel radius a. (*b*) Variation of the Fahraeus effect, indicated by H_T/H_D, with vessel radius a.

minimal value. The outer solutions corresponding to the cylindrical and hemispherical regions are matched through transition regions of lengthscale $\epsilon^{\frac{1}{2}}r_c$, where ϵr_c is the gap width, and tensions of order $\mu u_0 \epsilon^{-\frac{3}{2}}$ are generated in the membrane. At the front, this transition is monotonic, but the membrane bulges out at the rear transition region. As vessel radius increases, membrane tension decreases and the transition regions become wider and more pronounced. With further increases in radius, the tension in the rear transition region falls, until a radius is reached at which the tension is $o(\mu u_0 \epsilon^{-\frac{3}{2}})$. At this stage, a localized region of high curvature appears in the transition. If the tension in the rear transition region falls to $O(\mu u_0 |\log \epsilon|)$, the angle between the membrane and vessel wall changes by an $O(1)$ amount through the rear transition layer, so that the rear becomes less convex. The application of lubrication theory to the rear region in this case can be justified by a

comparison between the predictions of Stokes equation and lubrication theory in the case of flow in a corner.

In summary, our results show that red cell shape, rheological parameters, and distributions of pressure and membrane tension are highly sensitive to changes in diameter near the minimal value for intact passage of cells. These results, together with those of Secomb *et al.* (1986), show the wide variation of axisymmetric red cell shapes with capillary tube diameter.

This work was supported by National Institutes of Health grants HL34555, HL17421 and HL07249.

REFERENCES

BATCHELOR, G. K. 1967 *An Introduction to Fluid Dynamics*. Cambridge University Press.

BENDER, C. M. & ORSZAG, S. A. 1978 *Advanced Mathematical Methods for Scientists and Engineers*. McGraw-Hill.

BRETHERTON, F. P. 1961 The motion of long bubbles in tubes. *J. Fluid Mech.* **10**, 166–188.

CANHAM, P. B. & BURTON, A. C. 1968 Distribution of size and shape in populations of normal human red blood cells. *Circulation Res.* **22**, 405–422.

EVANS, E. A. & SKALAK, R. 1980 *Mechanics and Thermodynamics of Biomembranes*. Boca Raton, Florida: CRC Press.

FAHRAEUS, R. & LINDQVIST, T. 1931 The viscosity of blood flow in narrow capillaries. *Am. J. Physiol.* **96**, 562–568.

GAEHTGENS, P. 1980 Flow of blood through narrow capillaries: Rheological mechanisms determining capillary hematocrit and apparent viscosity. *Biorheol.* **17**, 183–189.

GRADSHTEYN, I. S. & RYZHIK, I. M. 1980 *Table of Integrals, Series and Products (Corrected and enlarged edition)*. Academic.

ÖZKAYA, N. 1986 Viscous flow of particles in tubes: Lubrication theory and finite element models. Ph.D. thesis, Columbia University, New York.

ÖZKAYA, N. & SKALAK, R. 1983 The steady flow of particles in a tube. In *1983 Advances in Bioengineering* (ed. D. L. Bartel), pp. 9–10. ASME.

PAPENFUSS, H.-D. & GROSS, J. F. 1981 Microhemodynamics of capillary networks. *Biorheol.* **18**, 673–692.

SECOMB, T. W. 1987 Flow dependent rheological properties of blood in capillaries. *Microvasc. Res.* **34**, 46–58.

SECOMB, T. W. 1988 Interaction between bending and tension forces in bilayer membranes. *Biophys. J.* **54**, 743–746.

SECOMB, T. W. & GROSS, J. F. 1983 Flow of red blood cells in narrow capillaries: role of membrane tension. *Intl J. Microcirc. Clin. Exp.* **2**, 229–240.

SECOMB, T. W., SKALAK, R., ÖZKAYA, N. & GROSS, J. F. 1986 Flow of axisymmetric red blood cells in narrow capillaries. *J. Fluid Mech.* **163**, 405–423.